# NOTES AND CORRESPONDENCE

## Thermodynamics of Eastern Mediterranean Rainfall Variability

GIDON ESHEL

*Department of the Geophysical Sciences, The University of Chicago, Chicago, Illinois*

BRIAN F. FARRELL

*Department of Earth and Planetary Sciences, Harvard University, Cambridge, Massachusetts*

14 February 2000 and 9 June 2000

ABSTRACT

This note focuses on thermodynamic changes caused by Eastern Mediterranean (EM) subsidence anomalies. Subsidence anomalies are shown to modulate EM-wide stability with respect to moist ascent. Additionally, convective available potential energy (CAPE) generation rates, as well as mean CAPE, change coherently during extreme EM rainfall anomalies. It is suggested that the resulting modulation of convective rain generation is the process directly responsible for the observed rainfall anomalies.

### 1. Introduction

Eshel and Farrell (2000, hereafter EF0) advance a simple explanation of Eastern Mediterranean (EM) rainfall variability in terms of subsidence anomalies associated with large-scale North Atlantic (NA) anomalies. What is missing from EF0 is a thermodynamic mechanism that directly causes observed EM rainfall anomalies. Presenting such a mechanism is the purpose of this note.

The EF0 mechanism is abbreviated below. Tropospheric mass variability forms a seasonally stationary wave pattern over the NA–Mediterranean sector. Nodes of opposite signs develop over Greenland–Iceland and the northern Mediterranean; Mediterranean-wide anticyclones (cyclones) accompany Greenland lows (highs). As the Mediterranean node is centered over the northern Adriatic region (well to the northwest of the EM), Mediterranean anticyclones (cyclones) correspond to EM northerlies (southerlies). These strong and persistent wind anomalies significantly modify heat advection. Because the (total, as well anomalous) flow is nearly thermally neutral (Rodwell and Hoskins 1996; EF0), enhanced subsidence heating accompanies anomalous cooling by horizontal winds, and cooling by ascent accompanies anomalous warming by horizontal winds. As the thermal structure changes relatively little, subsidence heating (cooling) anomalies are caused primarily by enhanced subsidence (ascent). Given the rapid decrease of specific humidity with height, subsidence anomalies strongly affect the lower-tropospheric moisture budget. The modified moisture advection is envisaged as the *indirect* cause of the EM rainfall anomalies. In this note we present a simple thermodynamic mechanism that may *directly* modify EM precipitation.

### 2. Data

A detailed discussion of the data can be found in EF0 and is not repeated here. Following EF0, the EM is defined as 32°–42°N, 22°–36°E. The time series of observed average rainfall in this region is shown in Fig. 1.

Tropospheric variables (winds, humidity, temperature) are taken from the National Centers for Environmental Prediction–National Center for Atmospheric Research reanalysis project (Kalnay et al. 1996); see EF0 for a discussion on the suitability of this dataset for the present purposes.

To characterize atmospheric states during EM rainfall extremes, we average atmospheric anomalies over the 30 months covering October–March of the five driest and five rainiest seasons after 1958 (the starting point of the reanalysis data; see EF0), shown by diamonds and circles in Fig. 1. We refer to the 30-month period of low EM precipitation as $P_L$, and to that of high EM precipitation as $P_H$.

*Corresponding author address:* Dr. Gidon Eshel, Dept. of the Geophysical Sciences, The University of Chicago, 5734 S. Ellis Ave., Chicago, IL 60637.
E-mail: geshel@uchicago.edu

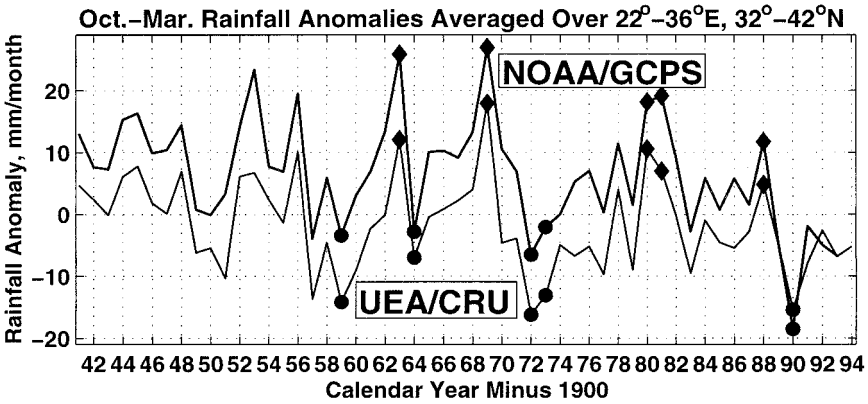


FIG. 1. Two gridded observational records of EM winter precipitation anomalies; thick line—National Oceanic and Atmospheric Administration's National Climatic Data Center/Global Climate Perspectives System (Baker et al. 1995; thin line—University of East Anglia/Climate Research Unit (Hulme 1992, 1994). The five rainiest and driest winters are denoted by diamonds and circles, respectively.

## 3. Rainfall modulation by anomalous subsidence

The thermodynamic mechanism we advance below to explain EM rainfall variability hinges on the well-established strong correlation between anomalous vertical motion and rainfall [e.g., Fulks (1935); Bannon (1948); reviews of the issue are found, e.g., in Palmén and Newton (1969), their section 12.6, particularly Eq. (12.4) and its approximations) and Emanuel (1994, section 16.2, Eq. (16.2.5)]. We apply the above relationship to specific extreme anomalies in the EM, and show strong and coherent modulation of EM moist static stability and convective available potential energy (CAPE) generation rates by subsidence anomalies. Taken together, the analyses of this note and EFO (in which the subsidence anomalies are analyzed in the context of hemisphere-scale flow anomalies) amount to a simple explanation of EM rainfall variability.

Since we focus on rainfall, for which ascending air parcels reaching saturation is a prerequisite, tropospheric static stability is of prime interest. The ambient static stability can be thought of as a potential barrier any ascending parcel must overcome in order to maintain its ascent and reach saturation. The energy required to overcome this barrier can be supplied by diabatic heating, or it can originate from the large-scale circulation. In any case, the more statically stable the atmosphere is, the more energy is required for ascent of a given mass, and hence the harder it is to generate rain. Figure 2 shows a very simple measure of static stability, the anomalous stratification with respect to moist ascent. {Since we consider rain-generating vertical motions, ascent is assumed to result in saturation and condensation; to account for latent heat release and the small effect of water vapor on density, in Fig. 2 we use the equivalent virtual potential temperature $\theta_{ve}$ [combining Wallace and Hobbs's (1977) Eq. (2.76), Emanuel's (1994) Eq. (4.4.14), and the reanalysis virtual air temperature].} Like EF0's figures, Fig. 2 shows very large and coherent signals, in which the $P_L$ configuration is roughly $P_H$'s opposite. Also, during a given extreme the east and west Mediterranean are antisymmetrical. EF0 attribute this antisymmetry to the fact that eastern- and western-Mediterranean meridional wind anomalies tend to be opposite in sign, thus being consistent with opposite subsidence anomalies. The stability anomalies are substantial; given climatological EM-mean winter $\theta_{ve}^{500} - \theta_{ve}^{925} = 3.6$ K, stability is 65% above climatology during $P_L$, and 30% below it during $P_H$; relative anomalies are similar in the upper troposphere (not shown). Consistent with the rain anomalies, the troposphere is more resistant to ascent (less likely to produce rain) during $P_L$ (Fig. 2a); the opposite holds during $P_H$ (Fig. 2b). Figure 2c shows that the relationship between EM rainfall and lower-tropospheric static stability is not limited to extreme conditions, with correlations significant at 0.05–0.01 throughout most of the region of interest (see EF0 for statistical methods). Together, Figs. 2a–c demonstrate that EM precipitation anomalies are intimately related to stability and vertical motion anomalies, the focus of this note.

While static stability affects rain generation in both stratus clouds (mostly due to warm front-related upgliding) and cumulus (cumulonimbus) towers, convective precipitation requires more than simple ascent. The potential for convective instability of the mean column can be quantified by calculating the work done by the buoyancy force on a saturated lifted air parcel—the column's mean CAPE. However, applying this argument to observations is not straightforward. Regularly convecting parts of the tropical atmosphere are believed by some to be essentially CAPE-free (Xu and Emanuel 1989). This has been attributed to extreme sensitivity of convection to conditional instability. From this notion, it follows that CAPE estimates are a poor predictor

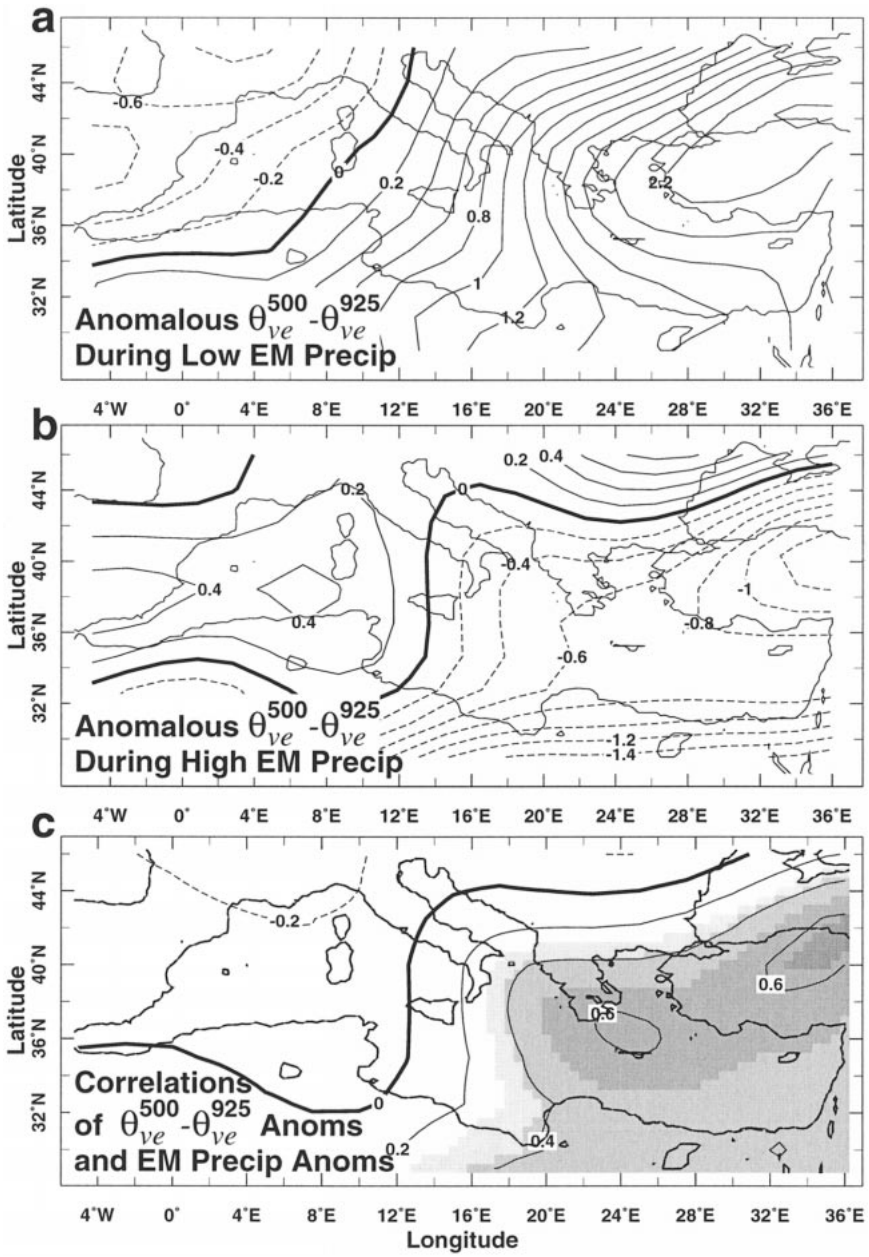


FIG. 2. A measure of lower-troposphere static stability, the difference in virtual equivalent potential temperature between 500 and 925 mb, in K (Kalnay et al. 1996). (a) and (b) During extreme EM rainfall events. (c) Temporal correlations over 1958–94 between stability anomalies (thus defined) and EM rainfall anomalies. Both fields are linearly best-fit detrended prior to correlation calculation. The four shadings denote *t*-test significance levels of 0.1, 0.05, 0.01, and 0.005. Contour interval is 0.2 K in (a) and (b), and 0.2 in (c).

of rainfall intensity. However, Williams and Renno (1993) have advanced an alternative view. Using three CAPE estimation methods and hundreds of tropical soundings spanning deep convective regions in the tropical Atlantic, the Amazon Basin, and the western Pacific, they obtained statistics indicating that $O(10^3$ J kg$^{-1})$ CAPE values are in fact very common in precipitating regions of the tropical atmosphere. If this result is borne out by future work, it suggests that CAPE and rainfall intensity *are* in fact statistically related. Thus the following calculation is not definitive, awaiting a satisfying resolution of the CAPE–rainfall interrelation problem.

Using Emanuel's (1994) Eqs. (6.1.5), (6.3.2), and (6.3.5) (with slight rearrangement),

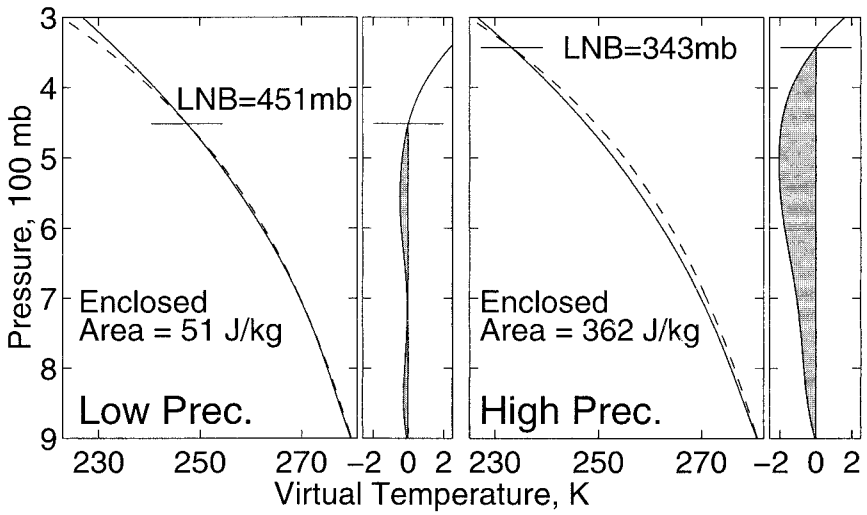


FIG. 3. Observed (Kalnay et al. 1996; solid) and calculated pseudoadiabatically lifted (dashed) $T_v$ profiles during EM rainfall extremes. The narrow panels to the right of the two main ones aid in discerning the differences between the two curves on each main panel; they use the calculated (dashed) curves as the zero line, and show only the deviation of the observed from the calculated. The heights of the LNB, the crossing points of the two curves, are indicated, as are the areas enclosed between the two curves from 900 mb to the LNB.

$$\text{CAPE} \equiv \int_{\text{TBL}}^{\text{LNB}} B\, dz = R_d \int_{\text{TBL}}^{\text{LNB}} \frac{\theta_v^p - \theta_v^a}{\theta_v^a} \frac{T_v^a}{p}\, dp, \quad (1)$$

where most of the notation is standard, TBL is the top of the boundary layer (here assumed 900 mb), $B$ is buoyancy [implicitly defined by Eq. (1), neglecting the effect of condensate on air density], superscripts $a$ and $p$ stand for ambient and pseudoadiabatically lifted parcel, and LNB is the level of neutral buoyancy (where $\theta_v^p \simeq \theta_v^a$). From the observed EM-mean 900–1300-mb $T_v^a$ profiles during $P_L$ and $P_H$, the pseudoadiabatic $T_v^p$ profiles during the two extremes are calculated,[1] the LNB is found, and the CAPE integral is evaluated numerically using Eq. (1). These profiles for both EM rainfall extremes are shown in Fig. 3. The time- and space-mean EM CAPE [Eq. (1)] is 51 J kg$^{-1}$ during $P_L$, and 362 J kg$^{-1}$ during $P_H$. On average, there is more than 7 times as much potential energy available for convection during $P_H$ than during $P_L$. This further supports the idea that EM rainfall extremes occur in response to (the very subtle) rearrangement of the vertical profiles of temperature and humidity of the spatial-mean column by anomalous subsidence.

While the above calculation represents the time-mean state, anomalous ascent induces a CAPE tendency, through a physical process best illustrated with the aid of Fig. 3. As the large-scale dynamics dictate mean ascent, the environmental air rises along a lapse rate $\Gamma$ representing some combination of the dry and moist adiabats. Unless a vast cloud covers the entire region (a practical impossibility, for which the distinction between environmental air and the ascending parcel is lost), $\Gamma > \Gamma_m$. The effect of this will be to shift the solid curves of Fig. 3 to the left, leaving the dashed curves intact. Because at any pressure this process operates $T_v^p - T_v^a$ increases, the area enclosed by the two curves between TBL and LNB [CAPE; Eq. (1)] increases, at a rate proportional to the ascent. Assuming $\omega \simeq -\rho g w$ and neglecting subcloud processes, adiabatic heating and horizontal dependence, this process is given approximately by

$$\left(\frac{\partial}{\partial t}\text{CAPE}\right)_{\text{ascent}} \simeq \int_{z_{\text{TBL}}}^{z_{\text{LNB}}} w\, N^2\, dz \simeq -\int_{p_{\text{TBL}}}^{p_{\text{LNB}}} \frac{R_d T_v}{p\theta_v} \omega \frac{\partial \theta_v}{\partial p}\, dp \quad (2)$$

[Emanuel's (1994) Eq. (14.2.13)], where $z$ and $p$ are height and pressure, $w$ and $\omega$ are the vertical velocities in these coordinates, $N^2$ is the buoyancy frequency, and $R_d$ is the dry-air gas constant. During subsidence, the situation is opposite and more extreme. Under subsidence, the environmental $\Gamma$ approaches $\Gamma_d \gg \Gamma_m$ (the latter characterizing the parcel, assuming it maintains its ascent against the subsidence opposition). Then while the thermal evolution of the parcel is unchanged (given

[1] Because the calculation solves for $T_v(p)$, it requires the moist adiabatic lapse rate $\Gamma_m$ [Emanuel's (1994) Eq. (4.7.3)], itself a function of temperature. Therefore at each $p$ increment (2 mb) the solution is sought iteratively. Starting from observed 900-mb $T_v^a$ and assuming an initial lapse rate, $T_v$ is evaluated, from which a new $\Gamma_m$ is computed, and the $T_v$ estimate is refined. When further iterations yield negligible $T_v$ changes, the calculation proceeds to the next $p$ level, until 300 mb.

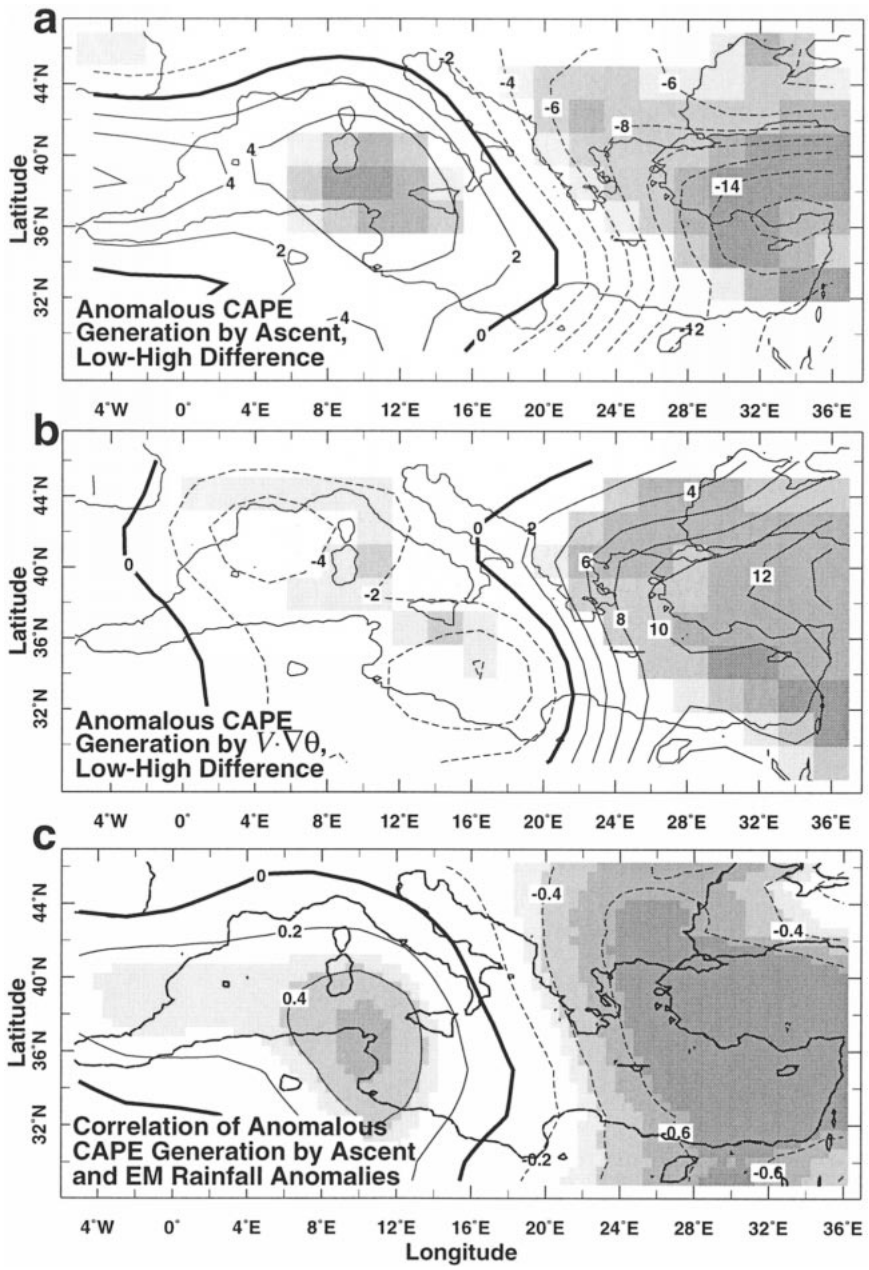


FIG. 4. The difference in CAPE generation rates by anomalous ascent (a) and horizontal motions (b) between $P_L$ and $P_H$, in J kg$^{-1}$ h$^{-1}$ (Kalnay et al. 1996); see text for details. (c) Correlations between CAPE generation rates by ascent (a) and EM rainfall anomalies (Fig. 1). Both records are linearly best-fit detrended prior to correlation calculation. The shadings denote significance levels of 0.1, 0.05, 0.01, and 0.005. Contour interval is 2 J kg$^{-1}$ h$^{-1}$ in (a) and (b), and 0.2 in (c).

by $\Gamma_m$), the air column within the vertical extent of the subsidence is pinned by the $\Gamma \simeq \Gamma_d$ to the high-$\theta$ air characteristic of the subsidence origin aloft. This pushes the thermal structure toward $T_v^a > T_v^p$, which increases the profile's negative area at the expense of the positive area [Emanuel's (1994) Eq. (6.3.6)], thus inhibiting convection. In addition, CAPE can be generated by horizontal motions, given approximately by

$$\left(\frac{\partial}{\partial t}\text{CAPE}\right)_{\text{horiz}} \simeq \int_{z_{\text{TBL}}}^{z_{\text{LNB}}} \frac{g}{\theta_v}\mathbf{V}\cdot\boldsymbol{\nabla}\theta_v\, dz \simeq -R_d \int_{p_{\text{TBL}}}^{p_{\text{LNB}}} \frac{T_v}{\theta_v p}\mathbf{V}\cdot\boldsymbol{\nabla}\theta_v\, dp \quad (3)$$

[Emanuel's (1994) Eq. (14.2.13)], where $g$ is the gravitational acceleration.

Figures 4a and 4b quantify these processes during the two EM precipitation extremes, while Fig. 4c extends the temporal coverage of Fig. 4a by including all years, not just extreme ones. Throughout most of the EM, the negative $P_L - P_H$ difference due to anomalous ascent (Fig. 4a) outweighs the positive difference due to $\mathbf{V} \cdot \nabla\theta_v$ by a small but systematic margin of 1–3 J kg$^{-1}$ h$^{-1}$. We suggest that this deficit is reflected in the results shown in Fig. 3, and can contribute to the rainfall modulation during $P_L$ and $P_H$. Together, Figs. 4a–c suggest that the rate of CAPE generation is highly relevant to rain production. During $P_H$, CAPE is generated in the EM troposphere at a mean rate of up to 2200 J kg$^{-1}$ month$^{-1}$ higher than during $P_L$. This again suggests that EM rainfall variability reflects anomalous motions; enhanced CAPE generation during $P_H$ yields more frequent and intense convection, while during $P_L$, CAPE generation is reduced, as is precipitation. The clear east–west antisymmetry of Figs. 4a–c further supports this interpretation, because of the subsidence antisymmetry, as discussed before.

## 4. Summary

We propose a simple physical mechanism linking EM rainfall anomalies directly to anomalous subsidence. We suggest that subsidence anomalies modify the mean column static stability and the CAPE generation rates. These processes alter the intensity of rain generation, and cause the observed EM rainfall anomalies. With EF0, where a mechanism linking NA climate variability to EM subsidence anomalies is presented, this amounts to a simple explanation of EM rainfall variability in terms of downstream effects of perturbed NA stationary waves.

*Acknowledgments.* GE thankfully acknowledges the generous support of the Woods Hole Oceanographic Institution. BF was supported by NSF ATM-96132362.

REFERENCES

Baker, C. B., J. K. Eischeid, T. R. Karl, and H. F. Diaz, 1995: The quality control of long-term climatological data using objective data analysis. Preprints, *Ninth Conf. on Applied Climatology,* Dallas, TX, Amer. Meteor. Soc., 150–155.

Bannon, J. K., 1948: Distribution of mass variations in atmospheric air columns. *Quart. J. Roy. Meteor. Soc.,* **74,** 57–66.

Emanuel, K. A., 1994: *Atmospheric Convection.* Oxford University Press, 580 pp.

Eshel, G., and B. F. Farrell, 2000: Mechanisms of eastern Mediterranean rainfall variability. *J. Atmos. Sci.,* **57,** 3219–3232.

Fulks, J. R., 1935: Rate of precipitation from adiabatically ascending air. *Mon. Wea. Rev.,* **63,** 291–294.

Hulme, M., 1992: A 1951–80 global land precipitation climatology for the evaluation of General Circulation Models. *Climate Dyn.,* **7,** 57–72.

——, 1994: Validation of large-scale precipitation fields in General Circulation Models. *Global Precipitation and Climate Change,* M. Desbois and F. Desalmand, Eds., Springer-Verlag, 466 pp.

Kalnay, E., and Coauthors, 1996: The NCEP/NCAR 40-Year Reanalysis Project. *Bull. Amer. Meteor. Soc.,* **77,** 437–471.

Palmén, E., and C. W. Newton, 1969: *Atmospheric Circulation Systems.* Academic Press, 603 pp.

Rodwell, M. J., and B. J. Hoskins, 1996: Monsoons and the dynamics of deserts. *Quart. J. Roy. Meteor. Soc.,* **122B,** 1385–1404.

Wallace, J. M., and P. V. Hobbs, 1977: *Atmospheric Science: An Introductory Survey.* Academic Press, 467 pp.

Williams, E., and N. Renno, 1993: An analysis of the conditional instability of the tropical atmosphere. *Mon. Wea. Rev.,* **121,** 21–36.

Xu, K. M., and K. A. Emanuel, 1989: Is the tropical atmosphere conditionally unstable? *Mon. Wea. Rev.,* **117,** 1471–1479.